UC Davis

UC Davis Previously Published Works

Title

Rotational multispectral fluorescence lifetime imaging and intravascular ultrasound: bimodal system for intravascular applications

Permalink

https://escholarship.org/uc/item/72p2m115

Journal

Journal of Biomedical Optics, 19(6)

ISSN

1083-3668

Authors

Ma, Dinglong
Bec, Julien
Yankelevich, Diego R
et al.

Publication Date

2014-06-04

DOI

10.1117/1.jbo.19.6.066004

Peer reviewed

eScholarship.org Powered by the California Digital Library
University of California

Journal of Biomedical Optics

SPIEDigitalLibrary.org/jbo

Rotational multispectral fluorescence lifetime imaging and intravascular ultrasound: bimodal system for intravascular applications

Dinglong Ma
Julien Bec
Diego R. Yankelevich
Dimitris Gorpas
Hussain Fatakdawala
Laura Marcu

SPIE

Rotational multispectral fluorescence lifetime imaging and intravascular ultrasound: bimodal system for intravascular applications

Dinglong Ma,[a] Julien Bec,[a] Diego R. Yankelevich,[a,b] Dimitris Gorpas,[a] Hussain Fatakdawala,[a] and Laura Marcu[a,*]
[a]University of California, Department of Biomedical Engineering, 451 Health Sciences Drive, Davis, California 95616
[b]University of California, Department of Electrical Engineering, 3101 Kemper Hall, Davis, California 95616

Abstract. We report the development and validation of a hybrid intravascular diagnostic system combining multispectral fluorescence lifetime imaging (FLIm) and intravascular ultrasound (IVUS) for cardiovascular imaging applications. A prototype FLIm system based on fluorescence pulse sampling technique providing information on artery biochemical composition was integrated with a commercial IVUS system providing information on artery morphology. A customized 3-Fr bimodal catheter combining a rotational side-view fiberoptic and a 40-MHz IVUS transducer was constructed for sequential helical scanning (rotation and pullback) of tubular structures. Validation of this bimodal approach was conducted in pig heart coronary arteries. Spatial resolution, fluorescence detection efficiency, pulse broadening effect, and lifetime measurement variability of the FLIm system were systematically evaluated. Current results show that this system is capable of temporarily resolving the fluorescence emission simultaneously in multiple spectral channels in a single pullback sequence. Accurate measurements of fluorescence decay characteristics from arterial segments can be obtained rapidly (e.g., 20 mm in 5 s), and accurate co-registration of fluorescence and ultrasound features can be achieved. The current finding demonstrates the compatibility of FLIm instrumentation with *in vivo* clinical investigations and its potential to complement conventional IVUS during catheterization procedures. © *2014 Society of Photo-Optical Instrumentation Engineers (SPIE)* [DOI: 10.1117/1.JBO.19.6.066004]

Keywords: fluorescence lifetime spectroscopy and imaging; intravascular ultrasound; bimodal catheter; intravascular imaging.

Paper 140097R received Feb. 17, 2014; revised manuscript received May 5, 2014; accepted for publication May 6, 2014; published online Jun. 4, 2014.

1 Introduction

Cardiovascular disease is the leading cause of death in developed countries.[1] Assessing the vulnerability of atherosclerotic plaques is an important part of clinical diagnostics. This involves the detection of plaque morphology and biochemical composition, as both have been shown to play a role in plaque rupture.[2] A few hybrid imaging techniques have proven effective in plaque characterization by combining structural imaging with biochemical imaging.[3] Near-infrared spectroscopy, known as being sensitive to presence of lipids in the plaque, has been combined with intravascular ultrasound (IVUS) and clinically applied to evaluate the lipid core of coronary atherosclerotic plaques.[4] Near-infrared fluorescence imaging (NIRF) has been used to detect plaque inflammation through activatable imaging agent,[5] which was co-registered with vessel morphology provided by IVUS.[6] A bimodal NIRF and optical coherence tomography (OCT) catheter have demonstrated *in vivo* imaging of stent microthrombus and inflammation.[7] Overall, these studies have demonstrated the high sensitivity of near-infrared spectroscopy/fluorescence imaging for specific biochemical features of atherosclerotic plaque, and their ability to operate through blood. However, NIRF-based techniques cannot resolve multiple chemical species in tissue simultaneously.

Techniques based on tissue autofluorescence excited in ultraviolet or visible range, albeit being challenged by the presence of blood in the optical field of view, are capable of interrogating multiple tissue chemical components simultaneously.[8–10] Instrumentation based on fluorescence lifetime spectroscopy and imaging techniques, in particular, has demonstrated the ability to evaluate arterial plaques' biochemical features, to stage atherosclerotic plaques based on their collagen, elastin, and lipid content.[11,12] Moreover, early studies showed their ability to operate intravascularly *in vivo* in the presence of blood flow.[13] Subsequently, in this study, we aim at evaluating a hybrid technique combining time-resolved fluorescence spectroscopy (TRFS) technique with IVUS.

In previous work, we showed that a point spectroscopy TRFS system can be adapted for multispectral fluorescence lifetime imaging (FLIm) through a helical scanning (rotation and pullback motion) of the artery using a side-viewing optical fiber.[14] Also, we developed a rotary multifunctional catheter that enables simultaneous multispectral FLIm and IVUS imaging,[15] and showed its ability to collect intravascularly robust bimodal data from large arteries (i.e., swine iliac arteries) *in vivo*.[16] However, these earlier prototypes using a rather large-diameter (7 Fr) catheter were not feasible for intravascular imaging of much smaller-diameter coronary arteries. Moreover, the interface between the TRFS and IVUS platforms was suboptimal for fast bimodal interrogation of long arterial segments.

The overall objective of current study is to demonstrate an automated and integrated FLIm–IVUS bimodal imaging

*Address all correspondence to: Laura Marcu, E-mail: lmarcu@ucdavis.edu

0091-3286/2014/$25.00 © 2014 SPIE

system compatible with *in vivo* intravascular fast imaging of coronary arteries. The intravascular diagnostic system reported here includes asynchronous FLIm–IVUS data acquisition and rotational catheter that enables automated helical (rotational and pullback) scanning of arterial vessels. The performance of this system was tested in a pig heart. The interface of FLIm and IVUS enables accurate direct axial co-registration and quasi-real-time image feedback from both imaging modalities. In addition, multiple facets of the rotational FLIm system performance, including the imaging speed, spatial resolution, efficiency, and lifetime measurement accuracy, were evaluated and reported here in order to understand the strength and limitation of the technique.

2 Bimodal Imaging System

The bimodal imaging system (Fig. 1) consists of a FLIm subsystem for detection and analysis of time-resolved fluorescence, an IVUS subsystem that provides ultrasound radiofrequency (RF) signal, an imaging catheter integrating the optical and ultrasound delivery-collection signal pathways, and a customized digitizer–controller module which controls the bimodal helical scanning, data acquisition and preprocessing, and a graphical user interface (GUI).

2.1 *FLIm System Configuration*

The FLIm system is based on a time-domain pulse sampling detection method which makes use of a multichannel wavelength selection module and fast electronics (detector and digitizer) to simultaneously resolve in multiple spectral bands the fluorescence excited state lifetime as reported previously by our group.[17,18] A fiberoptic-based multispectral FLIm system using this concept has been recently characterized in detail and also reported.[19] For the current study, a new wavelength selection module (WSM) was specifically designed with the goal of optimizing the efficiency of fluorescence excitation and collection while integrating all the components in a compact footprint. The excitation source is a pulsed diode-pumped mode-locked Ytterbium fiber laser with fundamental emission frequency of 1064 nm, 68-ps pulse width, and 6.8-μJ/pulse, providing variable repetition rate from 10 kHz to 1 MHz that is controlled by an acousto-optic pulse picker. A nonlinear optics module converts the fundamental frequency into 532-nm second-harmonic emission, which is later combined with the fundamental frequency to generate 355-nm third-harmonic emission with 80-ps pulse width and 350-nJ energy per pulse. The laser beam is coupled into a 200-μm core silica fiberoptic into the WSM and directed into an integrated rotary joint in the module through

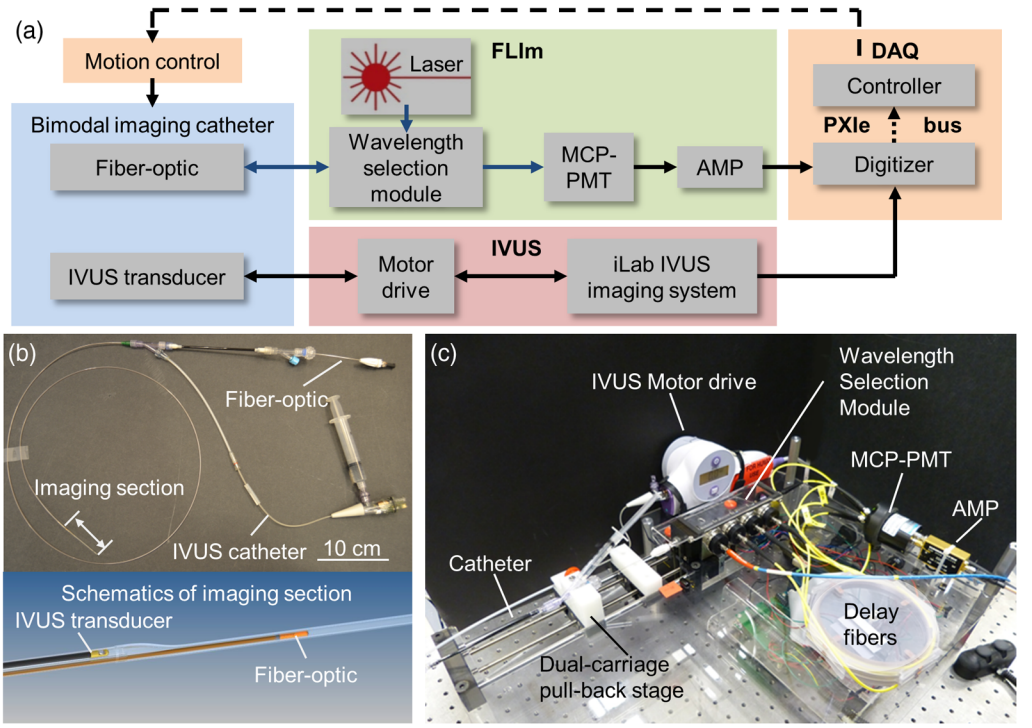

Fig. 1 Bimodal system schematic. (a) Fluorescence lifetime imaging (FLIm) subsystem: UV pulses from the laser are sent through a dichroic within the wavelength selection module (WSM) into the catheter's fiberoptic. The fluorescence emission is collected by the same fiberoptic, directed back into the WSM that spectrally resolves the emission, detected by a multichannel plate photomultiplier (MCP-PMT), and amplified by a preamplifier (AMP). IVUS subsystem: Boston Scientific iLab IVUS imaging system consists of an integrated motor drive that rotates a single element 40-MHz IVUS transducer (retrieved from Atlantis SR Pro coronary imaging catheter) at a constant speed of 1800 rpm. Bimodal imaging catheter: IVUS transducer and side-viewing fiberoptic integrated in a parallel design. [see (b)] Data acquisition (DAQ) and control module: Digitizer records analog signals from both FLIm and IVUS subsystems and upload the data to the embedded controller through PXIe bus. The controller communicates with motion controllers in charge of the catheter's helical scanning motion. (b) Completed assembly of the bimodal catheter and the imaging section. Fiberoptic and IVUS transducer enter the imaging section sequentially to perform helical scanning. (c) Photo of the compact assembly of catheter, motion control, and FLIm/IVUS system components.

a dichoic beamsplitter (>99% reflectance for 340 to 360 nm and >93% transmittance for 360 to 800 nm, z355rdc, Chroma Technologies, Bellows Falls, Vermont). The beam is then focused onto the excitation/collection fiber's proximal face by an achromatic lens (6.25-mm diameter, 12.5-mm effective focal length, TECHSPEC 87-327, Edmund Optics, Barrington, New Jersey) located in the rotary joint. The excitation light is then delivered to the sample through the side-viewing fiberoptic of the bimodal imaging catheter. The sample fluorescence is collected by this fiberoptic and sorted by a set of dichroic beamsplitters (Di01-R405-25x36, FF510-Di01-25x36, FF593-Di02-25x36, Semrock, Rochester, New York) and band-pass filters (FF01-390/40-25, FF01-452/45-25, FF01-542/50-25, FF01-629/53-25, Semrock, Rochester, New York) in order to spectrally resolve the fluorescence emission in four bands (390/40 nm, 452/45 nm, 542/50 nm, and 629/53 nm). The time-domain fluorescence signals are sequentially delayed with multimode silica fiber delay lines (400-μm core diameter, 0.22 NA, FVP400440480, Polymicro Technologies, Phoenix, Arizona) with 1, 10, 19, and 28 m lengths, generating ~46 ns incremental temporal delay between two consecutive channels. The temporally delayed multispectral fluorescence is detected by a multichannel plate (MCP) intensified PMT (R3809U-50, Hamamatsu, Japan) with a rise time of 183 ps. The MCP-PMT is powered by a 0 to 3000 V supply (Ortec 556, Oak Ridge, TN). An amplifier (C5594 Hamamatsu, Japan) with 1.5-GHz analog bandwidth is used to amplify the analog signal from the MCP-PMT by 36 dB before it can be recorded by the digitizer.

2.2 *IVUS System Configuration*

The IVUS system is based on a commercial 40-MHz IVUS system (iLab IVUS imaging system, Boston Scientific, Natick, Massachusetts) with minimal modifications to the original devices. The system includes the driving and receiving circuits of the transducer, data acquisition, and postprocessing devices, and a computer that runs commercial IVUS software and provides image display. Analog RF signal is transmitted from the transducer to the receiving circuits and amplified. It is accessible together with the trigger pulse for each A-scan through co-axial signal outputs. The IVUS images are acquired at 30 frames/s corresponding to a transducer rotation speed of 1800 rpm, with 256 A-scans per frame. The IVUS images are displayed in real time and can be recorded in compressed gray-level BMP image format while the system is continuously operating. However, in order to achieve synchronized bimodal data acquisition and perform RF analysis to the IVUS data, digitized RF data are recorded by digitizing the A-scan analog signal instead of the built-in image recording of the commercial system.

2.3 *Bimodal Data Acquisition*

The analog signals that convey fluorescence and ultrasound data are recorded by a high-speed digitizer (12.5 GS/s, 3 GHz, 8-bit, 512 Mbytes, PXIe-5185, National Instruments, Austin, Texas). The analog signals are sent into two separate input channels of the digitizer. The trigger signal of FLIm data acquisition is provided by a solid-state photo-detector (DET10A/M, Thorlabs, Newton, New Jersey) that detects light leakage from the second harmonic of the laser pulses (532 nm). The trigger signal of IVUS data acquisition is provided by the commercial IVUS system for each A-scan. However, the digitizer only provides one input channel for the trigger signals that synchronize the data acquisition. Therefore, a co-axial relay switch (DC to 18 GHz, 8762B co-axial switch, Hewlett-Packard, Palo Alto, California) driven by a digital I/O device (USB-6009, National instruments) is used to transmit alternative trigger signals to the trigger input of the digitizer. The digitizer is embedded in a device chassis with PXI express bus and connected to a controller (PXIe-8102, National Instruments). The controller is capable of running Windows 7 (Microsoft, Redmond, Washington) and platform software Labview (National Instruments) that enables system automation controls and online data processing and visualization.

2.4 *Bimodal Imaging Catheter*

A custom catheter coupled to the bimodal FLIm–IVUS imaging system enabled remote assessment of narrow tubular structures. This was achieved with a design where the fiberoptic and IVUS transducer are placed in parallel in a shaft large enough to accommodate both of them. However, they shared a narrower imaging section with a diameter of 3.5 Fr that is identical to the dimensions of the commercial 40 MHz IVUS catheter (Atlantis SE Pro2, Boston Scientific, Natick, Massachusetts). The shaft (Microspec, New Hampshire) made out of polybutylene terephthalate has an oval section with a largest diameter of 5 Fr. The imaging section (Vesta, California) is made of polymethylpentene (or TPX), chosen for its low sound impedance (<2 MRayls), very low fluorescence, and high transparency, making it particularly suitable for both ultrasound and fluorescence imaging. The ultrasound and optical channels consist of the imaging elements of the commercial IVUS 3-Fr catheter and a custom, total internal reflection, side-viewing fiber built around a UV-grade silica fiber optic (300-μm core diameter, 0.22 NA, 1.75 m long, FVP300330370, Polymicro Technologies, Phoenix, Arizona) with a polymethyl methacrylate (PMMA) cap [Fig. 1(b)]. Each modality can be moved into the imaging section and acquire data through helical scanning, while the other inactive channel is pulled back in the shaft.

2.5 *Helical Pullback Scanning Mechanism*

The helical scanning of the optical and ultrasonic channels in the bimodal imaging catheter requires rotation and pullback of each channel. The IVUS rotation is provided by the commercial motor drive, whereas the side-viewing optical fiber is connected to the integrated rotary joint of the WSM, which is driven by a high-speed servomotor (Maxon MCD EPOS, Sachseln, Switzerland) through a timing belt. The motor allows a wide range of rotation speed from 0 up to 12,000 rpm. The catheter sheath and the IVUS branch of the catheter are connected to a custom dual-carriage pullback stage driven by two stepper motors, controlled by a motion controller (PMX-2ED-SA, Arcus technology, Livermore, California) that communicates with the embedded controller in the digitizer. The sequential operation of the catheter is realized by relative motion between the catheter shaft, IVUS transducer, and the fiberoptics so that only one channel of the catheter is actively performing helical scanning in the imaging section. Similar to previous catheter design,[15] the pixel size or spatial sampling of FLIm along the axial and transaxial direction is determined by the helical scanning parameters and laser repetition rate.

2.6 *System Automation*

Automated system operation is implemented by a set of Labview-based software tools with GUI programmed in the controller to facilitate the intravascular imaging procedures using the bimodal imaging catheter. Bimodal imaging catheter alignment, automatic bimodal imaging sequence, and postimaging data analysis procedures are implemented in three software modules.

In preparation for the bimodal imaging sequence, the imaging plane of FLIm and IVUS imaging is manually aligned using a joystick control of the dual carriage stage. Once aligned, either channel can be precisely moved in different areas of the imaging section through automatic motion control. Real-time feedback of fluorescence signal is provided by the Labview interface and real-time IVUS image is provided by the computer display of the commercial IVUS system. Therefore, the catheter can examine the artery section for fluorescence features using FLIm or structure using IVUS subsystems independently.

The automatic bimodal helical scanning imaging sequence is defined by a series of pullback positions, rotation speed of fiberoptic, and the duration of data acquisition as a function of time in a GUI dialog window. Fiberoptic helical scanning can be configured with rotation speed from 0 up to 2400 rpm, pullback speed from 0 up to 4 mm/s, whereas FLIm multispectral data are acquired at 10 to 20 kHz rate with 2500 samples/data record, 80-ps sampling interval. Using 2400 rpm and 4 mm/s at 20-KHz laser repetition rate, the FLIm helical scanning provides a 100-μm axial sampling and 3-deg angular sampling. The IVUS transducer helical scanning uses 1800-rpm rotation speed (by default of the commercial system motor drive), 0 to 4 mm/s pullback speed while IVUS A-scan data are acquired at 7680 Hz (30 fps with 256 A-scans per frame) with 2000 samples per A-scan and 5-ns sampling interval.

At the highest helical scanning speed, the data acquisition during helical scanning for a 20-mm artery section takes 5 s for each modality to execute. In addition, the mechanical motion that advances/retracts sequentially the IVUS and FLIm catheter components into/from the imaging section requires 10 s for each modality. Switching from FLIm to IVUS requires reconfiguration of the digitizer and data transfer from the on-board memory of the digitizer to the random access memory (RAM) of the embedded controller, which in total account for 25 s.

Therefore, in current configuration, the entire FLIm–IVUS bimodal data acquisition sequence requires ~1 min that includes the data acquisition during helical scanning of both modalities, mechanical motion of the bimodal catheter, and FLIm data transfer into controller RAM. After bimodal data acquisition, the IVUS RF data are transferred from the on-board memory in to the controller RAM and saved immediately into the hard drive of the controller, which takes ~4 min. Then FLIm data in controller RAM are compressed by taking the average over four consecutive measurements and processed by the software to present preliminary results including the multispectral fluorescence transient waveforms and four channel *en face* fluorescence intensity images. After the FLIm data is reviewed, it is saved into the hard drive. The processing and saving of FLIm data takes less than 1 min. Thus, the bimodal data acquisition sequence including data saving and processing takes 6 min in total.

3 Bimodal System Characterization, Validation, and Performance

3.1 *FLIm System Spatial Resolution*

To determine the axial and transaxial spatial resolution of the side-viewing fiberoptic, a helical scanning FLIm was performed using a subresolution target composed of a layered structure with a nonfluorescence surface and a fluorescent inner layer. This was achieved by engraving the surface of the target that exposes the fluorescent substrate. The engraved line is placed parallel to the pullback direction to measure the transaxial resolution and perpendicular to the pullback direction to measure the axial resolution. The full-width at half-maximum (FWHM) of the intensity variation along the corresponding direction was used to define the resolution. The transaxial resolution measured in pixels was translated into angular scale (in degrees, under small angle approximation) and the axial resolution in pixels was directly converted into linear scale (in micrometers).

The spatial resolution (axial and transaxial) was found to be 160 μm and 14 deg, respectively, at 0-mm distance from the target and was found to be 355 μm and 14 deg, respectively, at 2-mm distance from the target.

3.2 *FLIm System Optical Throughput and Fluorescence Intensity Calibration*

To test the spectral efficiency of the WSM module and to generate intensity calibration factors, the optical throughput of each spectral channel was measured using a broadband LED light source emitting from near-UV to near-IR. To calculate the normalized transmittance of each WSM channel, the emission spectrum of the light source was measured by a fiber-coupled CCD array spectrometer (200 to 1100 nm, USB2000, Ocean Optics, Dunedin, Florida). The broadband optical radiation from the source was coupled into the WSM through a multimode fiber (300-μm core diameter, 0.22 NA, 1 m long, FVP300330370, Polymicro Technologies, Arizona) connected into the rotary joint. The light transmitted through the dichroic beamsplitters and filters as well as the delay fibers for each WSM channel was then detected by the spectrometer. The detected spectrum was normalized by the measured source spectrum to determine the optical transmittance spectrum. This measurement does not require knowledge of the exact emission spectrum of the light source or the spectral response of the spectrometer. The overall efficiency of converting collected photons to analog signal is given as a function of wavelength by multiplying the optical transmittance spectrum of each channel with the MCP spectral sensitivity curve. Fluorescence intensity calibration factors were calculated by taking the average efficiency values for each channel and normalizing it to the most efficient channel. These calibration factors were multiplied to the measured integrated intensity in order to recover the actual fluorescence intensity ratio between channels.

The transmittance spectra of the four WSM channels are shown in Fig. 2. The spectral width of each channel and the average transmittance within the spectral width are presented in Table 1. The transmittance of each channel was found to be uniform within its spectrum width and the average transmittance of all four channels were found to be similar. The fluorescence intensity calibration factors were calculated using the transmittance spectra and MCP spectral sensitivity curve. The results are presented in Table 1. Channel 2 was found to be

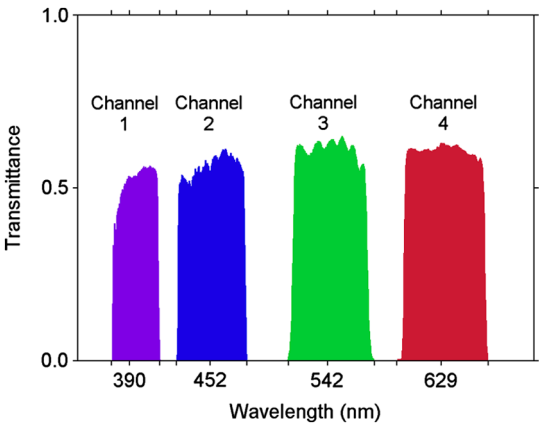

Fig. 2 Optical transmission efficiencies of the four channels of the WSM (average transmittance: channel 1 = 51.4%, channel 2 = 55.3%, channel 3 = 60.3%, channel 4 = 60.0%).

the most efficient channel and channels 1, 3, and 4 have relative efficiencies of 0.94, 0.77, and 0.52, respectively.

3.3 *Pulse Broadening Effect and System Impulse Response Function*

The fluorescence of biological fluorophores excited by a short (80-ps) laser pulse is typically a few nanoseconds. The measured fluorescence pulse transient, however, is broadened due to intermodal dispersion as it propagates through the multimode fibers and the finite bandwidths of the photodetector and electronic devices. Thus, the instrument impulse response function (iIRF) was measured to account for these pulse-broadening effects. This iIRF was used in the deconvolution of the fluorescence decay measurements. To determine the iIRF, a hemicyanine dye, 2-(p-dimethylaminostyryl)pyridylmethyl iodide (2-DASPI), dissolved in ethanol (1 mM, Sigma-Aldrich Corp.) with very short average lifetime (30 ps)[20] was excited by the 80-ps UV laser pulse. The emitted short (<100-ps) fluorescence pulse, measured via the system electronics, served as iIRF. The 2-DASPI in ethanol has a broad emission spectrum (covering channels 3 and 4) with a peak at 585 nm. The side-viewing optical fiber in the catheter was used to excite and collect the fluorescence of 2-DASPI. The delay fibers of 1, 10, 19, and 28 m

Table 1 Optical throughput and intensity calibration of the fluorescence lifetime imaging (FLIm) system.

Channel specifications (Center/ BW, nm)	Measured spectral widths (nm)[a]	Measured average transmittance	MCP spectral sensitivity (mA/W)[b]	Intensity calibration factors
390/40	35.5	51.4%	45.07	0.94
452/45	52.4	55.3%	45.60	1
542/50	55.9	60.3%	32.19	0.77
629/53	58.3	60.0%	21.91	0.52

[a]Full width at half maximum (FWHM) of the transmittance spectrum is used to determine the spectral widths.
[b]MCP cathode sensitivity at the center wavelength of the channel measured by the manufacturer.

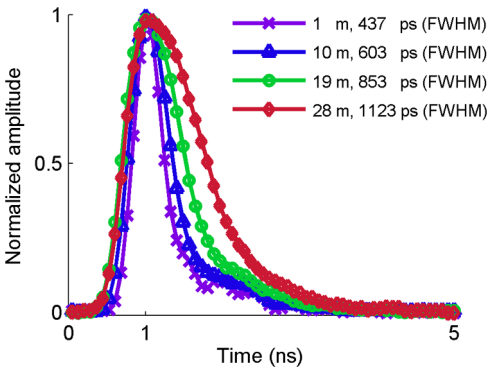

Fig. 3 Instrument impulse response functions (iIRFs) of the FLIm system of four different channels. A 300-μm core diameter side-viewing optical fiber was used for fluorescence excitation/collection. The pulse width values for each channel are shown in the legend.

were connected to the 542/50-nm channel one at a time in order to measure the iIRF for all four fiber lengths. A series of 1000 repeated measurements are taken for each delay fiber, and the recorded data waveforms are averaged to improve the signal-to-noise ratio (SNR).

The averaged iIRF pulses of the system for the four delay fibers are given in Fig. 3. The FLIm system presents 437, 603, 853, and 1123 ps FWHM of the iIRF for channels 1, 2, 3 and 4, respectively.

3.4 *Lifetime Measurement Error Analysis*

To retrieve the fluorescence decays and estimate the average lifetimes, the measured iIRF was numerically deconvolved from measured fluorescence pulse transient. In brief, the fluorescence decay pulse can be modeled as a convolution of the fluorescence impulse response (fIRF) and the instrument impulse response:

$$f(t) = \int_{-\infty}^{\infty} \mathrm{fIRF}(\tau) \cdot \mathrm{iIRF}(t-\tau)\mathrm{d}\tau + \varepsilon(t),$$

where $\mathrm{fIRF}(t)$ is the fluorescence emission excited by short laser pulse before being broadened by the system, $\mathrm{iIRF}(t)$ is the instrument impulse response that accounts for all broadening to fIRF by the system, and $\varepsilon(t)$ is the additive noise mixed in the signal. A least-square deconvolution algorithm based on nonparametric model using Laguerre expansion was used to determine the fIRF.[21]

Two types of errors are likely to affect the estimated lifetime values. Random errors can be generated by the noise in the fluorescence measurements. Systematic errors can be introduced by the multispectral fluorescence detection method using optical delay lines; in particular, when the fluorescence decay lasts longer than the temporal separation between optical channels. The systematic and random errors introduced by the FLIm system were evaluated using both simulated and experimental data.

To evaluate the random errors, experimental multispectral FLIm data acquired from *ex vivo* coronary artery [as presented in section below (see Fig. 7(d))] was analyzed to quantify the random error in fluorescence lifetime measurement and its correlation with measurement noise level. Results were compared to simulated data presented in previous study showing a negative correlation between the raw signal's SNR and the standard deviation (SD) of average lifetime.[21] Briefly, the simulated

fluorescence signal (fIRF) was generated by mixing an arbitrary number of exponential decay functions with various lifetimes and convolved with a short pulse iIRF, before adding Gaussian white noise with 20 to 50 db SNR. Then, the average lifetimes of the simulated signals were estimated using deconvolution algorithm mentioned earlier. For the multispectral FLIm data, the SNR of each pixel in the *en face* image was calculated based on the signal power spectral density (PSD) of each channel, and the noise PSD was quantified from the noise section ahead of the first channel fluorescence signal in time domain. The average lifetime images of *ex vivo* coronary artery were manually segmented to retrieve 5×5-pixel (0.5 mm×14.4 deg) ROIs. The SD of the lifetime values within the ROI was calculated and plotted as a function of the average SNR within the ROIs. The relationship between SD and SNR based on simulation and experimental data is demonstrated in Fig. 4. The negative correlation between lifetime SD and SNR demonstrated by experimental data agrees with the trend (fitted to an exponential model with SNR in decibels) presented by the simulated data in a previous report.

Systematic lifetime measurement error can be caused by a set of physical constraints to the fIRF, which was initially enforced to improve the robustness of deconvolution algorithm against noise as follows:

$$\begin{cases} \lim\limits_{t\to\infty} \mathrm{fIRF}(t) = 0 \\ \mathrm{fIRF}'(t) < 0 \\ \mathrm{fIRF}'(t) > 0 \end{cases} \quad 0 \le t < \infty.$$

These constraints require the fIRF to be convex, monotonic decreasing, and converging to zero. However, when the fluorescence decay lasts longer than the duration in which the fluorescence signal was recorded (46 ns/channel), the computational constraints enforcement will lead to a premature truncation of the decay and hence underestimating the average lifetime. The lifetime estimation error caused by this effect was evaluated by simulating the fIRF by a set of monoexponential decay functions (1- to 8-ns lifetimes) and the iIRF by a Gaussian pulse with FWHM of 600 ps, which is close to the FWHM of the measured channel 2 iIRF. The convolution of fIRF and iIRF was truncated into various time durations (40, 45, and 50 ns) and processed by the deconvolution algorithm to evaluate the average lifetime measurement error using various truncation parameters. The deconvolved lifetime as a function of the lifetimes of the monoexponential decay functions for three different truncation parameters in the simulation is shown in Fig. 5. The FLIm system performs closest to the 45-ns curve, which presents less than 0.06 ns errors for decays with average lifetime smaller than 5 ns. The trend from 40 to 50 ns truncation duration shows that the error can be decreased by increasing the truncation duration, which is eventually associated with the length differences between optical delay lines.

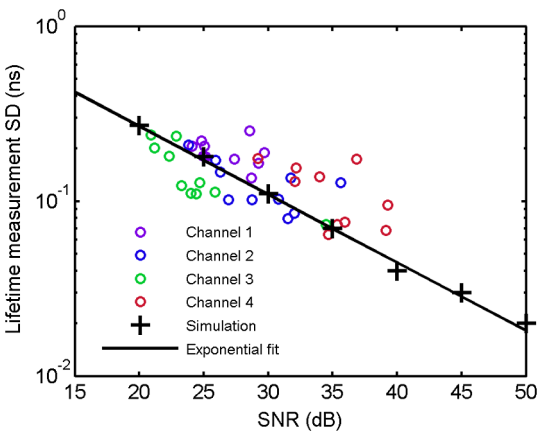

Fig. 4 Theoretical and experimental correlation of signal-to-noise ratio (SNR) and lifetime measurement standard deviation (SD). *Ex vivo* coronary artery average lifetime images (Fig. 7(d)) were manually segmented to select regions of interest (ROIs) for each channel in which the average SNR and lifetime SD is calculated and plotted as scatter plot. Lifetime estimation SD of simulated data generated by random multiexponential decay model with different levels of Gaussain white noise (black cross) was fitted to an exponential function of SNR (black solid line) and agreed with the experimental data.

3.5 *FLIm System Validation in Tubular Phantom*

A fluorescent PMMA tubular phantom [Fig. 6(a)] was used to evaluate the ability of FLIm system to acquire data from cylindrical structures with small inner diameter (3 mm) and to simultaneously resolve the fluorescence emission of multiple fluorophores. To generate additional fluorescence contrast and structural features, a drug-eluting stent (DES) (TAXUS Liberté Atom Paclitaxel-Eluting Coronary Stent System, Boston Scientific, Natick, Massachusetts) was marked with green and pink fluorescent paint (Scribbles, Fresno, California) at the extremities and deployed in the lumen of the phantom. Then, the imaging section of the catheter was introduced into the lumen using a catheterization guide wire. A 20-mm-long helical scan with 1200 rpm rotation and 2 mm/s pullback speed was performed to acquire multispectral FLIm images from the lumen.

The fluorescence emission spectra of the DES coating, green and pink fluorescent marker and the fluorescent PMMA tube were measured with an existing fluorescence spectroscopy system[22] including a scanning monochromator and served as reference spectra. The normalized spectra of these fluorescent entities are shown in Fig. 6(b). They display a relatively broad spectral width with emission peaks at 445 nm (DES coating), 505 nm (green paint), 540 nm (PMMA), and 595 nm (pink paint). Thus, the DES coating is expected to be seen in channels 1, 2, and 3; the green paint marker in channels 2 and 3; the PMMA phantom background fluorescence primarily emits in channel 3, and the pink paint marker emits mainly in channel 4.

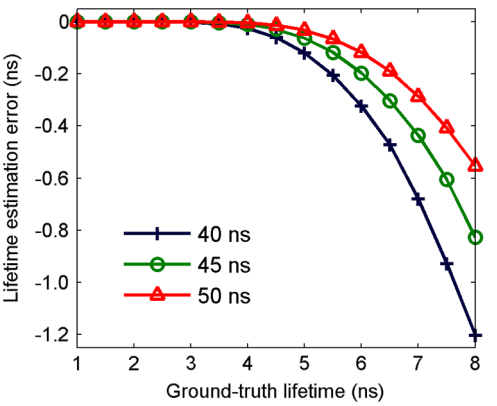

Fig. 5 Lifetime estimation error as a function of the ground-truth lifetimes in the simulation study. The legend shows the truncation window lengths.

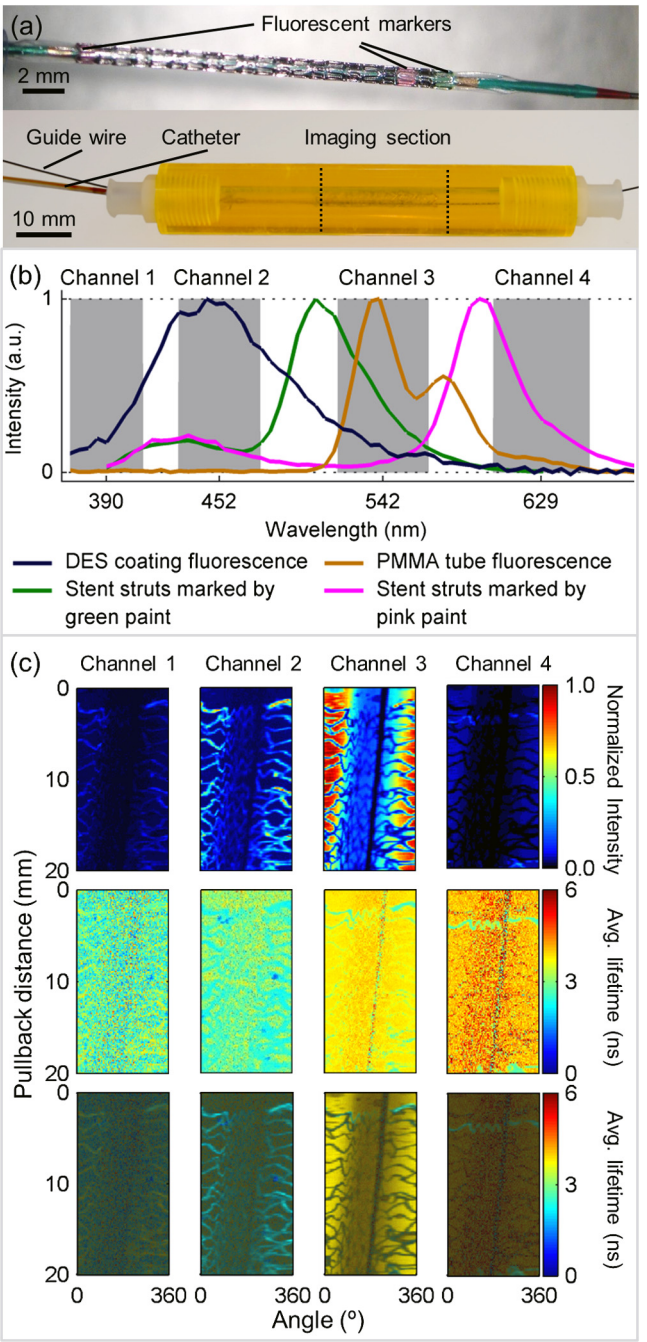

Fig. 6 (a) Tubular phantom made of fluorescent polymethyl methacrylate (PMMA) with 3-mm lumen. The drug-eluting stent (DES) was marked with fluorescent paint and deployed in the lumen. (b) Fluorescence intensity spectra of phantom components and the spectral bands of the WSM. (c) Fluorescence intensity images, average lifetime images, and intensity weighted lifetime images of four spectral channels.

The fluorescence intensity, lifetime images, and intensity weighted lifetime images of the phantom are presented in Fig. 6(c). The intensity images indicate that the fluorescence emission of the four fluorescent entities cannot be clearly resolved based on intensity alone. For example, in channel 3, the green paint emission cannot be resolved from that of the PMMA emission. Also, although particular fluorescent entities can be spectrally resolved in their respective channels (e.g., DES coating spectrally resolved in channels 1 and 2 and PMMA tubular structure resolved in channel 3), the intensity of the fluorescence is nonuniformly distributed across the surface.

The lifetime images, on the other hand, present a uniform average lifetime for each fluorescent entity for a sufficient SNR. The average lifetime values of various fluorescent entities presented in the current and the following section are mean values extracted from 10 different micro-ROIs containing more than 50 pixels on the corresponding FLIm features. For example, the DES coating showed uniform lifetime values (2.4 ± 0.2 ns) in channel 2 where the channel matches its fluorescence emission peak. In channel 1, the fluorescence signal from the DES coating is low and the lifetime values retrieved were more randomized as expected from the correlation between lifetime measurement errors versus SNR demonstrated earlier. The stent struts painted with fluorescent markers (2 to 4 mm and 19 to 20 mm along pullback direction) with average lifetimes of 2.8 ± 0.2 ns (green in channel 3) and 2.5 ± 0.2 ns (pink in channel 4) are clearly distinguished from the fluorescence background of PMMA tube (3.7 ± 0.1 ns in channel 3 and 3.6 ± 0.2 ns in channel 4). The side-band emission of the fluorescent entities also contributed to some features, such as the partial stent structures in channel 3 generated by the DES coating providing average lifetimes lower than the surrounding PMMA background.

The intensity weighted lifetime images combined the intensity and lifetime information by modulating the opacity of the pseudocolored average lifetime images using the corresponding intensity images, thus providing the maximum discrimination of fluorescence features. The lifetime contrast was enhanced by the intensity contrast while the uniformity of the same fluorescent entities is maintained. For example, in channel 2, the randomized lifetime background was suppressed by the intensity weighting, and the uniform lifetime contrast of the DES coating was maintained. In channel 3, the full stent structure is not clear in average lifetime image due to overwhelming background fluorescence from PMMA tube, whereas the stent struts marked by green paint are not clear in intensity image. Both the full stent structure and the green paint–marked stent struts can be resolved in the intensity weighted lifetime image.

3.6 *Bimodal System Validation in Swine Heart (Coronary Arteries)*

An intact swine heart was used as *ex vivo* platform for testing the bimodal system ability to operate and record data from coronary arteries which are similar in size with those of human heart. A fresh (<1 h after animal death) pig heart was used for intracoronary imaging. The blood was removed from the arteries by flushing saline through the lumen and a catheterization guide wire (0.014" 190 cm, Pilot 150, Abbott Vascular, Temecular, CA) was introduced through the left anterior descending (LAD) coronary artery of the heart [Fig. 7(a)]. First, IVUS imaging of the coronary vessel was performed in order to locate a 3-mm-diameter section. Then, a drug-eluting stent (DES) (CYPHER Sirolimus-eluting Coronary Stent, Cordis Corporation, Miami Lakes, Florida) marked with green and pink fluorescent paint (Scribbles, Fresno, California) was deployed in the previously identified artery section to provide additional fluorescence contrast and structural features to the background of healthy coronary vessel [Fig. 7(b)]. Thereafter, the bimodal catheter was introduced into the artery. The stented section was located using real-time IVUS imaging of the commercial system and a 20-mm FLIm–IVUS sequential helical scan

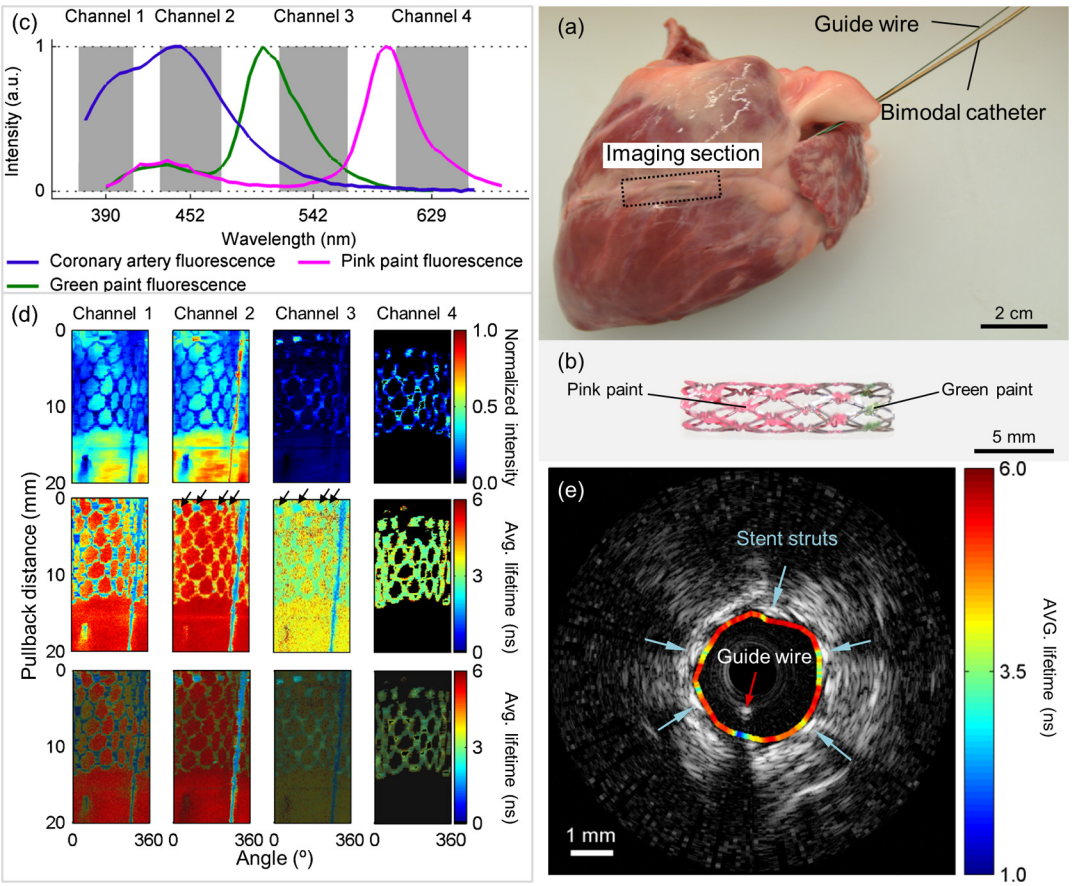

Fig. 7 Bimodal imaging of *ex vivo* coronary artery with fluorescence marked drug-eluting stent (DES) deployed in the lumen. (a) Overview of the pig heart with catheter inserted in the left anterior descending artery. (b) Close-up of the drug-eluting stent showing the painted sections. (c) Fluorescence intensity spectra of fluorescent paints, arterial tissue, and the spectral bands of the WSM. (d) Fluorescence intensity images, average lifetime images, and intensity weighted lifetime images of four spectral channels showing the stent structure (green paint marked struts are pointed by arrows) and the guide wire (vertical line). (e) IVUS cross-sectional image of the vessel with fluorescence lifetime registered over the arterial wall. Stent struts and guide wire can be identified with both FLIm and IVUS contrast.

was executed (FLIm: 2400 rpm, 4 mm/s; IVUS: 1800 rpm, 4 mm/s). This bimodal pullback imaging sequence was repeated five times at the same section in the artery to acquire multiple sets of data. After removing the catheter from the artery, the arterial lumen was opened to retrieve the DES. The fluorescence emission spectrum of the coronary lumen tissue and the fluorescent green and pink paint on the DES was also measured with the fluorescence spectroscopy system including a scanning monochromator as noted above and served as reference spectra. The FLIm *en face* images and IVUS cross-section images were co-registered along the axial direction based on the initial alignment of fiberoptic and transducer imaging planes. The angular co-registration was based on the angular location of the guide wire observed in both modalities. The IVUS image was manually segmented to retrieve the vessel lumen in order to register the FLIm average lifetime values in the cross-section.

The reference fluorescence emission spectra of the coronary artery and the paint markers are shown in Fig. 7(c). The coronary artery autofluorescence, primarily generated by collagen and elastin, is presented in channels 1 and 2 and is spectrally separated from the fluorescence of the green and pink paint marker on the DES, mainly present in channels 3 and 4, respectively.

The multispectral fluorescence intensity, average lifetime images, and the intensity weighted lifetime images of the artery lumen are depicted in Fig. 7(d). For a very small portion (<1%) of the pixels in the images, the fluorescence signal detected by the MCP exceeded the input range of the digitizer which renders the average lifetime estimation inaccurate. Thus, these pixels were excluded from data analysis. The coronary artery shows uniform lifetime distribution in channels 1, 2, and 3, with mean average lifetime of 5.3 ± 0.2 ns, 5.5 ± 0.1 ns, and 3.7 ± 0.3 ns, respectively. The arterial tissue contains multiple fluorophores that contribute to the signal in different WSM channels, and so the artery lifetime presented in channels 1 and 2 can be dominated by combined collagen and elastin fluorescence. Elastin is known as having a broad emission spectrum[10,23] may contribute to the fluorescence emission in channel 3 and exhibits a shorter lifetime. Measurements of collagen and elastin using a very similar multispectral FLIm system can also be found in Ref. 19. The stent areas marked with green and pink paint were not differentiated in channel 1, both showing low lifetime (1 to 2.5 ns). It is possible that the two paint materials share some common compounds that fluoresce in channel 1, as indicated by the overlapped TRFS spectra. The green paint marked stent struts show consistent lifetime in channels 2 and 3 (2.1 ± 0.2 ns and

2.3 ± 0.2 ns, respectively), whereas they present no signal in channel 4 as expected from the control measurement [Fig. 7(c)]. The pink paint marked stent area also shows consistent mean lifetime in channels 3 and 4 (2.8 ± 0.2 ns and 2.9 ± 0.2 ns, respectively). The catheter guide wire, which can be differentiated in channels 1, 2, and 3 from both intensity and lifetime images, was used as a fiducial marker for co-registration.

The co-registered FLIm and IVUS cross-section image of the *ex vivo* coronary artery is presented in Fig. 7(e). The stent struts in the IVUS image are featured by hyperechoic sectors along the vessel lumen boundary. From the *en face* fluorescence lifetime values, the painted stent struts can be distinguished by relatively lower lifetime compared to the coronary artery fluorescence. Six stent struts can be observed along each rotation of the helical scanning. One of these struts was overshadowed by the guide wire, so that only five of them are identified in the co-registered cross-section. The IVUS and FLIm contrasts of the stent struts overlapped angularly very well in the co-registered image.

4 Discussion

In this study, we developed a robust and compact rotational FLIm–IVUS imaging system compatible with intravascular imaging of coronary arteries. The integration of FLIm and IVUS subsystems was implemented for both catheter deployment and data acquisition. The system incorporates a custom build small profile (3.5 Fr imaging section) bimodal imaging catheter. The data acquisition of FLIm and IVUS is combined sequentially using a high-speed digitizer. To our knowledge, this study demonstrates for the first-time bimodal FLIm–IVUS imaging of coronary arteries in an intact pig heart (comparable in size with human heart) and co-registration of biochemical features derived from FLIm with structural information derived from conventional IVUS.

Intravascular diagnostics require instrumentation capable of providing information about arterial wall characteristics in near-real time. Thus, the ability to sample/scan a few centimeters arterial segments in short time (few tens of seconds) is of critical importance for the FLIm system. Moreover, the presence of blood can affect the optical signal, thus clearance of blood can occur only briefly within the limits imposed by physiological conditions, typically <20 s (e.g., bolus injection used in conventional OCT or other procedures).[24,25] Subsequently, a high-speed FLIm data acquisition during helical scanning is required. The fiber laser used in this study provides sufficient repetition rate (10 kHz to 1 MHz) while the MCP-PMT provides continuous detection. The fast light source and photodetector support the digitizer operation at its maximum data recording rate of 400 kHz (data records/second) if not limited by other factors. Currently, the limiting factor of FLIm data acquisition speed is the rotation speed of the fiberoptic, i.e., maximum of 2400 rpm for stable rotation. Significantly faster rotation speed of the fiberoptic, e.g., 4800 rpm or higher, may cause nonuniform velocity profile duration rotation and hence distortion in the FLIm images. At the highest rotation speed, the maximum memory of the digitizer (512 Mb) enables FLIm data recording over a 50-mm artery segment with Nyquist spatial sampling (80 to 178 μm $\times$ 7 deg) based on the spatial resolution. However, imaging of such long artery segments is not necessary in practical application. Therefore, the large memory size of the digitizer can be used to over-sample a shorter artery segment. The FLIm system reported here can helically scan a 25.6-mm artery segment with 100 μm $\times$ 2.88 deg spatial sampling at 2400 rpm rotation, 4 mm/s pullback, and 20 kHz data acquisition rate. Overall, the FLIm imaging pullback sequence takes up to 6.4 s, which is compatible with the bolus injection used in clinical settings. While the current 6-min total time required to execute an entire FLIm–IVUS bimodal imaging sequence including saving both FLIm and IVUS data is relatively long and not compatible with clinical applications, it is acceptable for *in vivo* preclinical applications in animal models of atherosclerosis (e.g., swine). In future developments, the data saving time can be significantly reduced by using solid-state memory in the embedded controller of the digitizer. Online lifetime data analysis can also be implemented to provide multispectral FLIm images before data storage.

In addition, in the current study, we aimed at testing the FLIm operational system parameters in conditions that are permitted for human use. One goal was to minimize the fluence of excitation laser light at the tissue level while increasing the optical system fluorescence light collection (throughput) and increase the SNR. The maximum permissible exposure (MPE) of skin to UV light is regulated by the ANSI standard. This is given by $0.56t^{0.25}$ J/cm^2 at 355 nm, where t is the total exposure duration. Depending on the helical scanning and laser parameters, the MPE can be as low as 3.3 mJ/cm^2 (at 2400 rpm, 20 kHz), corresponding to 150 nJ/pulse delivered to the tissue, whereas the pulse energy delivered through the system can be much higher. In an earlier version of the instrument, we relied on an optical rotary joint (60% transmission) that operated separate from the WSM.[15] By integrating the rotary joint within the WSM, we removed most of the losses and increased the excitation/collection efficiency by 180% with respect to the previous version. In order to further optimize the fluorescence collection efficiency of the WSM, the delay fibers have a larger core diameter (400 μm) than the core diameter (300 μm) of the side-viewing fiberoptic of the catheter. The optical throughput measurement has demonstrated that all four channels of the WSM have >50% light transmittance.

The multispectral FLIm imaging of tubular phantom (Fig. 6) and coronary artery (Fig. 7) demonstrated that their fluorescence emission can be rapidly resolved spectrally and temporally within one catheter pullback and that the distribution of distinct fluorescent constituents can be also spatially resolved. For example, fluorescence features with spectral overlap (e.g., green paint and PMMA tube) and similar lifetime (DES coating, green paint, and pink paint) can be differentiated by combining the time- and spectral-domain information in the multispectral FLIm images. A similar scenario can be expected for measurements of diseased arterial wall. As demonstrated in previous studies,[11] fluorescence parameters derived from time-resolved fluorescence measurements conducted in distinct spectral channels allows for discrimination of distinct type of plaques, including collagen-rich from lipid-rich plaques as well as from normal arteries that have the fluorescence emission dominated by elastin. Nevertheless, the spatial resolution of the FLIm system is limited by the fiberoptic excitation-collection geometry, so spatial convolution effect is expected to play a role in depicting fluorophore distribution. The value of a particular pixel in the multispectral average lifetime image is actually the average lifetime given by all the fluorophores covered by the beam profile centered at the pixel coordinates. For example, the average lifetime value of what seems to be the stent struts, which in fact is a subresolution object, is the weighted average between the background and the paint fluorescence depending on their contribution to the signal.

The lifetime measurement error analysis demonstrated that a systematic error can occur when measuring long-lived fluorophores. However, current WSM with a 46-ns time decay window presents very low error for lifetime values shorter than 5 ns. Furthermore, such errors can be significantly reduced by extending the length of the optical delay fibers so that it no longer affects lifetime estimation results. The random error observed in the experimental data is very well correlated with the SNR, which means that controlling the signal's SNR is sufficient to provide precise fluorescence lifetime measurements. While for time-correlated single photon counting (TCSPC) method, the SNR (or number of counts) is very well correlated with the relative error of lifetime measurement,[26] the pulse sampling detection method used by the current system cannot precisely control the SNR and hence the lifetime measurement error. The introduction of additional noise by the electrical system (i.e., amplifier and digitizer) reduces the SNR from the shot noise limit which follows Poisson statistics. On the other hand, the pulse sampling method precisely controls data acquisition time for each fluorescence decay, whereas TCSPC methods cannot determine the data acquisition time *a priori*. There is a fundamental difference between the two methods: the pulse sampling is a speed prioritized method, whereas TCSPC is an accuracy prioritized method. Nevertheless, since the measurement accuracy of the current system still increases as SNR improves, the largest lifetime measurement error can be confined by setting the lowest SNR in the image through increasing laser output power or MCP gain.

The integration of the FLIm and IVUS subsystems was achieved without major modification of the IVUS system. Current design takes advantage of exiting commercial IVUS catheter assembly and electronic systems for proof-of-concept studies. The FLIm fiberoptic was rotated by an independent motor drive and advanced in the narrow imaging section after the IVUS image was taken. While current bimodal catheter (parallel configuration) is not totally practical as it requires sequential advancement in the imaging components (US transducer and side-viewing fiberoptic), it allowed for immediate demonstration of hybrid imaging approach and its ability to provide co-registration of biochemical data (fluorescence contrast) with structural data (ultrasound contrast). The direct digitization of IVUS analog signals allows for synchronization of automated motion and IVUS data acquisition, which was used to achieve axial co-registration. Future engineering of a co-axial catheter configuration along with a motor drive that can rotate both the US transducer and the fiberoptic simultaneously will not only allow for simultaneous acquisition of IVUS and FLIm data and reduce the overall data acquisition time but also provide a direct co-registration of FLIm and IVUS image.

While the current bimodal imaging system has demonstrated feasibility for intravascular interrogation of narrow coronary arteries, clinical translation of such system faces a few additional challenges. First, the system would need to operate in blood flow. Blood has a high optical absorption in both UV and visible wavelength range where the arterial wall fluoresces.[27] The use of bolus injection of flushing agent with proper optical property has the potential to address this challenge. Current FLIm system is capable of acquiring data in 5 s (20-mm pullback) thus compatible with the timeframe of a conventional bolus injection, typically in the range of 1.5 to 3.5 s[24] or 11.5 to 16.5 s.[25] Second, vessel motion and deformation caused by heartbeat and breathing could adversely affect the co-registration between IVUS and FLIm. The current study was performed using a bimodal imaging catheter with parallel configuration where the helical scanning and data acquisition for the two modalities were done sequentially. Therefore, the vessel morphology as well as the distance between the catheter and the vessel wall might be different during pullbacks (IVUS versus FLIm). The benchtop experiments, as conducted in this study, allowed us to account for potential geometrical changes between pullbacks. This would not be possible when the measurements are conducted during cardiac motion. As discussed earlier, a co-axial catheter configuration enabling the FLIm and IVUS catheter components to rotate and acquire data simultaneously will maintain the co-registration of the two modalities even during vessel wall motion, and thus be able to overcome such challenges. Third, currently the lifetime data analysis is performed offline while the online software provides only spectral intensity information of the vessel, so the complete diagnostic information is only available after the catheterization procedure is done. While such delay is acceptable for preclinical animal studies, online lifetime data analysis should be provided for clinical application to facilitate making diagnostic decisions. Future development of software will include lifetime analysis algorithms implemented on parallel computing architecture to achieve quasi-real-time lifetime data analysis and display.

5 Conclusions

This article reports the design and engineering of a bimodal intravascular imaging system combining rotational FLIm and IVUS techniques. This system allows for helical scanning of narrow arterial vessels, sequential acquisition of time-resolved fluorescence data and ultrasonic data, and co-registration at the luminal surface between fluorescence lifetime images with ultrasonic images. The functionality of this hybrid system was tested *ex vivo* in explanted intact swine hearts, experiments that demonstrated the ability of this bimodal system to operate reliably in coronary arteries and to provide registered biochemical and structural information about these vessels. The fluorescence excitation and collection efficiency of the rotational FLIm system were optimized using a small-footprint wavelength selection module specifically designed for intravascular imaging. This system is capable of temporarily resolving the fluorescence emission simultaneously in multiple spectral channels in a single pullback sequence. Importantly, this system enables rapid and accurate measurements of fluorescence emission from an arterial segment (e.g., 20 mm in 5 s). Current results demonstrate the compatibility of FLIm instrumentation with *in vivo* clinical investigations and its potential to complement conventional IVUS during catheterization procedure.

Acknowledgments

This work was supported by National Institutes of Health (NIH) grant R01-HL67377 and the training program in molecular imaging grant 5T32EB003827.

References

1. D. Lloyd-Jones et al., "Heart disease and stroke statistics-2010 update a report from the American Heart Association," *Circulation* **121**(7), E46–E215 (2010).
2. A.V. Finn et al., "Concept of vulnerable/unstable plaque," *Arterioscler. Thromb. Vasc. Biol.* **30**(7), 1282–1292 (2010).

3. C.V. Bourantas et al., "Hybrid intravascular imaging," *J. Am. College Cardiol.* **61**(13), 1369–1378 (2013).
4. C. Simsek et al., "The ability of high dose rosuvastatin to improve plaque composition in non-intervened coronary arteries: rationale and design of the Integrated Biomarker and Imaging Study-3 (IBIS-3)," *Eurointervention* **8**(2), 235–241 (2012).
5. F.A. Jaffer et al., "Real-time catheter molecular sensing of inflammation in proteolytically active atherosclerosis," *Circulation* **118**(18), 1802–1809 (2008).
6. G. Mallas et al., "Improving quantification of intravascular fluorescence imaging using structural information," *Phys. Med. Biol.* **57**(20), 6395–6406 (2012).
7. H. Yoo et al., "Intra-arterial catheter for simultaneous microstructural and molecular imaging in vivo," *Nat. Med.* **17**(12), 1680–U202 (2011).
8. A. Zukauskas et al., "Characterization of biological materials by frequency-domain fluorescence lifetime measurements using ultraviolet light-emitting diodes," *Opt. Mater.* **30**(5), 800–805 (2008).
9. A. Christov et al., "Optical detection of triggered atherosclerotic plaque disruption by fluorescence emission analysis," *Photochem. Photobiol.* **72**(2), 242–252 (2000).
10. J. M. I. Maarek et al., "Time-resolved fluorescence spectra of arterial fluorescent compounds: reconstruction with the laguerre expansion technique," *Photochem. Photobiol.* **71**(2), 178–187 (2000).
11. L. Marcu et al., "Detection of rupture-prone atherosclerotic plaques by time-resolved laser-induced fluorescence spectroscopy," *Atherosclerosis* **204**(1), 156–164 (2009).
12. L. Marcu et al., "Discrimination of human coronary artery atherosclerotic lipid-rich lesions by time-resolved laser-induced fluorescence spectroscopy," *Arterioscler. Thromb. Vasc. Biol.* **21**(7), 1244–1250 (2001).
13. D.N. Stephens et al., "Intraluminal fluorescence spectroscopy catheter with ultrasound guidance," *J. Biomed. Opt.* **14**(3), 030505 (2009).
14. H.T. Xie et al., "Multispectral scanning time-resolved fluorescence spectroscopy (TRFS) technique for intravascular diagnosis," *Biomed. Opt. Express* **3**(7), 1521–1533 (2012).
15. J. Bec et al., "Design, construction, and validation of a rotary multifunctional intravascular diagnostic catheter combining multispectral fluorescence lifetime imaging and intravascular ultrasound," *J. Biomed. Opt.* **17**(10), 106012 (2012).
16. J. Bec et al., "Multispectral fluorescence lifetime imaging system for intravascular diagnostics with ultrasound guidance: in vivo validation in swine arteries," *J. Biophoton.* **7**(5), 281–285 (2013).
17. Y. Sun et al., "Simultaneous time- and wavelength-resolved fluorescence spectroscopy for near real-time tissue diagnosis," *Opt. Lett.* **33**(6), 630–632 (2008).
18. Y. H. Sun et al., "Dynamic tissue analysis using time- and wavelength-resolved fluorescence spectroscopy for atherosclerosis diagnosis," *Opt. Express* **19**(5), 3890–3901 (2011).
19. D. R. Yankelevich et al., "Design and evaluation of a device for fast multispectral time-resolved fluorescence spectroscopy and imaging," *Rev. Sci. Instrum.* **85**(3), 034303 (2014).
20. J. Kim et al., "Photophysical properties of hemicyanine dyes intercalated in Na-fluorine mica," *J. Phys. Chem. A* **104**(7), 1388–1392 (2000).
21. J. Liu et al., "A novel method for fast and robust estimation of fluorescence decay dynamics using constrained least-squares deconvolution with Laguerre expansion," *Phys. Med. Biol.* **57**(4), 843–865 (2012).
22. S. Yang et al., "Development of a dual-modal tissue diagnostic system combining time-resolved fluorescence spectroscopy and ultrasonic backscatter microscopy," *Rev. Sci. Instrum.* **80**(6), 065104 (2009).
23. L. I. Laifer et al., "Biochemical basis for the difference between normal and atherosclerotic arterial fluorescence," *Circulation* **80**(6), 1893–1901 (1989).
24. G. J. Tearney et al., "Three-dimensional coronary artery microscopy by intracoronary optical frequency domain imaging," *JACC Cardiovasc. Imaging* **1**(6), 752–761 (2008).
25. F. Prati et al., "From bench to bedside: a novel technique of acquiring OCT images," *Circ. J.* **72**(5), 839–843 (2008).
26. H. C. Gerritsen et al., "Fluorescence lifetime imaging in scanning microscopy," in *Handbook of Biological Confocal Microscopy*, 3rd ed., J. B. Pawley, Ed., pp. 516–534, Springer, New York, NY (2006).
27. S. A. Prahl et al., "Optical absorption of hemoglobin," Oregon Medical Laser Center, Oregon, Tech. Rep. (1999).

Dinglong Ma received his BS in optical engineering in 2010 from Zhejiang University, China. He is currently a PhD candidate in the Department of Biomedical Engineering at the University of California, Davis. His research interests include time-resolved fluorescence imaging and spectroscopy, and their clinical instrumentation.

Julien Bec received a MS degree in automotive engineering from Centrale Lyon and Politecnico di Torino and several years as an R&D engineer working on mechanics, automation, energy transfer and thermochemistry for automotive manufacturers, including Ferrari. He is currently a development engineer involved in biomedical optics research focusing on the development and fabrication of novel fluorescence lifetime imaging devices and nuclear imaging instrumentation.

Diego R. Yankelevich received his MS and PhD degrees in electrical and computer engineering from the University of California, Davis, in 1989 and 1993, respectively. He is currently an adjunct professor with the Department of Electrical and Computer Engineering, University of California. His research interests include organic nonlinear optical materials, ultrashort-pulse nonlinear microscopy, sum-frequency spectroscopy of nonlinear biological tissues and instrumentation for biomedical time-resolved fluorescence spectroscopy and photoacoustic imaging.

Dimitris Gorpas is a postdoctoral fellow in biomedical engineering at University of California, Davis. He received his PhD in engineering from National Technical University of Athens, Greece. His research focuses on medical image and signal processing, fluorescence lifetime imaging, fluorescence molecular imaging, light transport in scattering dominated media, three-dimensional surface and volume reconstruction and visualization.

Hussain Fatakdawala received his BS in biomedical engineering in 2009 from Rutgers University, New Brunswick, New Jersey, USA. He is currently pursuing his PhD in biomedical engineering at the University of California Davis, Davis, California, USA. His research interests include fluorescence lifetime imaging and ultrasound for assessment and characterization of atherosclerotic plaques, oral carcinoma and engineered tissues.

Laura Marcu is a professor of biomedical engineering and neurological surgery at University of California Davis. She received her doctorate degree in biomedical engineering in 1998 from the University of Southern California, Los Angeles. Her research interests include fluorescence-based techniques for biomedical diagnostics and clinical translation of optical technologies.